Nanotoxicology, June 2013; 7(4):389–401

ISSN: 1743-5390 print / 1743-5404 online
DOI: 10.3109/17435390.2012.665506

informa
healthcare

A standardised approach for the dispersion of titanium dioxide nanoparticles in biological media

Julian S. Taurozzi[1], Vincent A. Hackley[1] & Mark R. Wiesner[2]

[1]*National Institute of Standards and Technology, Material Measurement Laboratory, MD, USA and* [2]*Department of Civil and Environmental Engineering, Duke University, Durham, NC, USA*

Abstract

We describe a comprehensive optimisation study culminating in a standardised and validated approach for the preparation of titanium dioxide (TiO_2) nanoparticle dispersions in relevant biological media. This study utilises a TiO_2 reference nanomaterial based on a commercially available powder that has been widely examined in both acute and chronic toxicity studies. The dispersion approach as presented here satisfies four key harmonisation requirements not previously addressed: (1) method transferability, based in part on the use of a sonication energy calibration method that allows for power measurement and reporting in a device-independent manner; (2) optimisation of sonication parameters and thorough method validation in terms of particle size distribution, pH, isoelectric point, concentration range and batch variability; (3) minimisation of sonolysis side effects by elimination of organics during sonication and (4) characterisation of nanoparticle agglomeration under various dispersion conditions by use of laser diffraction spectrometry, an *in situ* size characterisation technique that provides advantages over other techniques more commonly employed within the context of nanotoxicology (e.g. dynamic light scattering). The described procedure yields monomodal, nanoscale, protein-stabilised nanoparticle dispersions in biological media that remain stable for at least 48 h (acute testing timeframe) under typical incubation conditions.

Keywords: Nanomaterial, agglomerate, bovine serum albumin, toxicology, suspension

Introduction

Experimental studies designed to evaluate the environmental, health and safety (EHS) risks of engineered nanomaterials (ENMs) invariably require the dispersion of the test material in a matrix of relevance to the *in vitro* or *in vivo* study (e.g. cell culture media, buffer or natural water). However, unless protected in some manner (e.g. by a surface coating), nanoparticles will typically destabilise and form agglomerates when introduced to test media, due to charge screening by electrolytes or interaction with medium components (Schulze et al. 2008; Jiang et al. 2009).

Particle agglomeration upon introduction to relevant media complicates both the determination of the delivered *nanoparticle* dose and the discrimination of *size-specific* particle effects, since the target (cell or animal model) is simultaneously exposed to both nanoscale particles and microscale agglomerates of the test material. Agglomeration may change the net reactivity of the nanoparticles making up such assemblages, when nanoparticle surfaces participate in reactions (Hotze et al. 2010), and ENMs may undergo uncontrolled surface modifications upon introduction to the test medium, such as the formation of a protein corona in serum containing biological media (Lundqvist et al. 2008; Aggarwal et al. 2009) or the adsorption of natural organic matter, present in most environmental matrices (Lin et al. 2010; Zhang et al. 2009). The preparation of nanoscale, stable and monomodal ENM dispersions with a well-defined surface in relevant biological media is thus a fundamental challenge that must be addressed in order to ensure the reproducibility, reliability and relevance of ENM risk assessment studies.

There is growing consensus within the risk assessment community on the need for standardised and validated dispersion methods to ensure reliable and reproducible results, and to enable the advancement of risk assessment research (National Science and Technology Council 2007; National Science and Technology Council 2008). In particular, the interest in nanoscale TiO_2 is driven in part by its substantial production volume and its use in both consumer products (e.g. sunscreens) and industrial applications (Pew 2011; Robichaud et al. 2009; Kuempel & Ruder 2006; U.S. Environmental Protection Agency 2010). Published studies on the potential hazards associated with nanoscale TiO_2 have yielded mixed results and do not provide a clear consensus (Warheit et al. 2007; Kuempel & Ruder 2006); however, there is sufficient evidence that nanoscale-specific

Correspondence: Vincent A. Hackley, National Institute of Standards and Technology, Material Measurement Laboratory, MD 20899-8520, USA. Tel: +301 975 5790. E-mail: vince.hackley@nist.gov

(Received 31 October 2011; accepted 1 February 2012)

biological effects exist for this material (Krysanov et al. 2010; Sass 2007; Johnston et al. 2009; Yang et al. 2009).

While a wide variety of agents have been studied for nanoparticle stabilisation in biological media, proteins are an especially attractive option due to their biocompatibility and the fact that proteins can mimic the actual corona coating that particles spontaneously acquire when introduced to biological matrices (MacCuspie et al. 2011; Porter et al. 2008; Sager et al. 2007; Schulze et al. 2008). In particular, several studies have investigated the stabilising effect of proteins on TiO_2 nanoparticles: Ji et al. (2010) studied the agglomeration of TiO_2 nanoparticles in a variety of biological matrices, showing a significant improvement of particle stability when supplementing the medium with albumin-rich solutions (bovine serum albumin – BSA and foetal bovine serum – FBS); Porter et al. (2008) developed a protein-rich medium for TiO_2 dispersion and demonstrated its efficacy as a biocompatible surrogate medium for pulmonary toxicity studies, and Allouni et al. (2009) studied the agglomeration and sedimentation of TiO_2 nanoparticles in biological media, demonstrating a significant reduction in particle agglomeration in the presence of proteins. Additional studies have focused on optimising TiO_2 dispersion procedures. For instance, Bihari et al. (2008) systematically studied dispersion and stabilisation sequence parameters in biological media, Sager et al. (2007) conducted microscopy imaging studies to determine the effectiveness of different protein-medium combinations for dispersing TiO_2 in biological matrices and Kim et al. (2010) proposed an electro-spray-based approach for the dispersion of airborne TiO_2 nanoparticles.

Building on this previous work, we herein address yet unresolved obstacles for the dispersion of nanoscale TiO_2 in biological media, with the aim of advancing the harmonisation and reliability of studies focused on the evaluation of biological and environmental hazards related to TiO_2 nanoparticles. In this work, we describe a standardised approach for the preparation of protein-stabilised TiO_2 nanoparticle dispersions in relevant biological media via sonication, in a manner that (1) enables inter-laboratory transferability and reproducibility, (2) optimises sonication dispersion parameters towards the attainment of the smallest achievable nanoscale dimensions while minimising the potential for sonolysis artefacts and (3) validates nanoparticle and dispersion parameters under relevant incubation conditions over time.

This approach is demonstrated using National Institute of Standards and Technology (NIST) Standard Reference Material (SRM) 1898, a traceable TiO_2 test material based on a widely used and industrially relevant commercial powder (Evonik-Degussa 2010; OECD 2008)[1], two broadly used and representative biological media – namely phosphate-buffered saline (PBS) and Dulbecco's Modified Eagle Medium containing 10% foetal bovine serum (DMEM-FBS), and bovine serum albumin (BSA), a thoroughly studied and widely available protein with numerous biological assay applications, as the model stabilising agent for the preparation of dispersions in the two selected media. Key parameters considered critical for the validation of stability and compatibility of dispersions used in risk assessment studies, namely isoelectric point (IEP), pH and particle size distribution (PSD), are characterised. Moreover, we employ orthogonal *in situ* measurement techniques for PSD validation.

The application of the dispersion approach demonstrated here yields monomodal TiO_2 nanoparticle dispersions, characterised by mean particle diameters of ≈ 75 nm (in PBS) and ≈ 83 nm (in DMEM-FBS) and pH values from 7.2 to 7.4 (in PBS) and 7.8 (in DMEM-FBS). The dispersions retain their stability (characterised by the PSD) and pH in the test media and under typical incubation conditions for at least 48 h – a timeframe relevant to acute toxicity tests. The approach is validated for several TiO_2 production lots, including a test material recently utilised in the Organization for Economic Cooperation and Development (OECD) Sponsorship Program for the Testing of Manufactured Nanomaterials (2008).

Materials and methods

The dispersion and characterisation approaches described in this work are demonstrated by use of NIST SRM 1898 and validated using additional production lots from the same commercial source. All tested nanomaterial powders (NIST SRM and additional lots) correspond to a commercially available TiO_2 powder commonly referred to in the literature as "Degussa P25" or simply "P25" (AEROXIDE TiO_2 P25 powder, Evonik Degussa GmbH, Germany). SRM 1898 is a nanocrystalline material with a mean crystallite size of approximately 24 nm (refer to the Supporting Information for more details). Relevant physicochemical property data (e.g. crystal structure, surface area, *etc.*) for SRM 1898 are available on the SRM certificate (NIST 2012), while a generic description of P25 is provided in the Supporting Information. Type I biological-grade de-ionised (DI) water (18.2 MΩ·cm) was used in the preparation of test samples; biological grade implies sterility and absence of endotoxin contamination.

BSA (>99%, reagent grade, lipid and IgG free) powder (SeraCare Life Sciences, MA, USA) and FBS (Gemini Bio-Products, CA, USA) were used as protein sources. Calcium- and magnesium-free PBS was prepared by dilution in DI water of a 10× concentrate (HyClone Laboratories, UT, USA), followed by filtration through 0.1 μm pores using a sterile filter. DMEM-FBS was prepared by adding FBS (10% volume fraction) into sterile DMEM (Mediatech, Inc., VA, USA) containing 4.5 g/L glucose and sodium pyruvate without L-glutamine or phenol red, and added penicillin–streptomycin, fungizone antimycotic and glutimax supplement. The pH of the media was adjusted by use of 0.1 mol/L NaOH or HCl aqueous solutions.

Sonication was performed using a Branson 450 analogue sonicator (Branson Ultrasonics Corp., CT, USA) outfitted with a $^1/_2$ inch (1.3 cm) diameter titanium horn with a removable flat tip; the horn was immersed directly into the suspension. The temperature probe used for sonication energy calibration was an Extech HD 200 temperature meter and datalogger coupled to a type-K immersion temperature probe.

[1]The identification of any commercial product or trade name does not imply endorsement or recommendation by the National Institute of Standards and Technology.

Dynamic light scattering (DLS) measurements were performed using a Zetasizer Nano ZS (Malvern Instruments Inc., MA, USA) operating in backscatter mode with a scattering angle of 173°. Samples were analysed in 1.5 mL disposable cuvettes by dilution in DI water (up to 1 mL total volume) to achieve an appropriate light scattering level. The measurement protocol used in this method is described elsewhere (Hackley & Clogston 2007). For each sample, measurements were performed in triplicate, with the number and duration of sub-measurements for each run determined automatically by the instrument's software. A non-negatively constrained least squares inversion algorithm, provided by the vendor, was used to generate intensity and volume-based PSDs by application of the Mie scattering model and using a particle refractive index of 2.5. A regularisation parameter of 0.01 was selected, with data parsed over 70 bins.

Laser diffraction spectrometry (LDS) measurements were performed using a Partica LA-950 V2 (Horiba Instruments Inc., CA, USA). Differential volumetric PSDs were calculated by application of the Mie scattering model, with a particle refractive index of 2.5. Measurements were conducted by introducing the sample into a stirred 15 mL quartz cell containing the same medium as the tested sample, until an acceptable blue line transmittance level was attained (between 70% and 90% transmittance). The measurement baseline was determined using the appropriate medium as the blanking solution. Further instrument details are offered in the Supporting Information.

X-ray disc centrifuge (XDC) measurements were performed using a BI-XDCW (Brookhaven Instruments Corporation, NY, USA) equipped with a standard 10 cm disc. For measurements, 25 mL of a 10 mg/mL sample was loaded into the disc and spun at 3500 rpm (58.3 Hz) for 32 min. The PSD was calculated using the radial scanning mode and the Stokes equation for laminar flow particle settling under a centrifugal field.

Electron micrographs were obtained using a field emission scanning electron microscope (FE-SEM, S-4700, Hitachi, CA, USA), operating at a 10 kV accelerating voltage in ultrahigh image resolution mode. Samples were prepared by electrostatic deposition onto a (1 × 1) cm section diced from a silicon wafer (PCA 10361, p-type, University Wafer, MA, USA). Suspensions were placed in contact with the substrate's native oxide surface and incubated for 1 min, followed by rinsing with filtered DI water to remove unattached particles. FE-SEM samples were not sputter coated, allowing for the direct observation of the native particles.

The mean electrophoretic mobility was measured by phase analysis light scattering using the Zetasizer Nano ZS and a dip cell equipped with palladium electrodes. The sample was contained in a standard 10 cm disposable cuvette.

For the determination of the IEP, zeta potential was measured as a function of pH, by acid–base titrations of TiO_2 suspensions. Further details on the titration method can be found in the Supporting Information. Sample pH was determined using an Orion 3-Star pH meter (Thermo Electron Corp., MA, USA) equipped with an InLab Semi-Micro pH electrode (Mettler Toledo, OH, USA) and an automatic temperature compensation probe (Orion 927006MD, Thermo Electron Corp., MA, USA).

Unless otherwise noted, uncertainties reported for measurement values are based on a type A analysis (Taylor & Kuyatt 1994). The standard deviation (or standard uncertainty) was calculated under repeatability conditions for triplicate independent samples. The standard deviation was multiplied by a coverage factor $k = 2$. The resulting uncertainty value is referred to as the expanded uncertainty.

Definitions of key terms, as used in the present context, are provided in the supplemental information.

Results and discussion

The overall strategy employed in this work for the preparation of dispersions in the tested biological media has three basic procedural components: (1) pre-dispersion by sonication of the ENM powder in biologically sterile purified water, (2) post-sonication introduction of proteins as the stabilising agent and finally (3) preparation of dispersions in the relevant test media by direct introduction of the protein-stabilised ENM aqueous concentrate. The summarised results and associated discussions are organised following these procedural steps.

Preliminary considerations

PSD measurements

DLS is widely used for the *in situ* determination of mean particle size or PSD of nanoparticle suspensions prepared in various test media; however, in the present work we utilise LDS as the principal size characterisation technique. Our rationale is as follows: (1) LDS, like DLS, is an *in situ* measurement, with measurement durations comparable with DLS. However, LDS allows for the measurement of a much wider size range (roughly 10 nm to 3000 μm) as compared with DLS, enabling the detection of agglomerated fractions that are beyond the typical DLS measurement range; (2) DLS is strictly applicable to particles that undergo Brownian diffusive motion with negligible settling during the timeframe of the measurement. Therefore, DLS can underestimate or neglect the presence of large agglomerates, even within the DLS detection range, as a result of rapid settling or very slow diffusive motion (Hackley & Clogston 2007). Conversely, LDS relies solely on the scattering properties of the particles, and the use of a stirred or recirculating cell prevents settling of agglomerates during measurement; (3) For particles with sizes above the Rayleigh scattering regime (e.g. micrometre-scale agglomerates), the scattering envelope becomes increasingly non-isotropic, and the widely used fixed-angle DLS instrument (typically 90° or 173°) becomes less reliable for the accurate determination of PSDs. By comparison, LDS employs multiple detectors at forward and backscatter angles, enabling the full characterisation of multimodal samples with coexisting nano- and microscale components; and (4) LDS accommodates higher sample concentrations than typically acceptable for DLS measurements, thus mitigating the need for sample dilution. Additionally, LDS offers another advantage over DLS in the present context, as it permits the direct measurement of

Table I. Calorimetrically measured *delivered* sonication power corresponding to different sonicator settings. Uncertainties are based on triplicate determinations at each setting.

Setting	Power (W)
1	9.3 ± 1.2
3	31.9 ± 3.5
5	52.3 ± 1.0
8	97.0 ± 4.4
10	120.8 ± 18.6

samples in their native complex biological media, without the need for dilution of the sample in water or removal of solution-phase proteins. It must be noted that while LDS was used in optimisation tests due to the above-mentioned advantages over DLS for the characterisation of polydisperse PSDs in complex media, two additional sizing techniques – namely DLS and XDC – were used for the evaluation of monomodal samples (i.e. post-optimisation), as discussed in the PSD validation section.

Sonolysis effects

Based on a survey of recent literature, a typical procedure used for dispersing ENM dry powders in biological or environmental media involves adding the components directly to the medium, followed by sonication for a specified period of time at an intensity level deemed appropriate for the particular test sample. This approach, however, is prone to the sonolytical degradation of organic molecules (Naddeo et al. 2007; Basedow & Ebert 1979; Kawasaki et al. 2007) – major constituents of relevant media used in such studies – and can consequently lead to artefacts that could impact the observed biological response. Therefore, the first step towards minimising the potential for undesired sonolysis effects adopted for the approach proposed in the present work was to sonicate the test powder in purified water, in the absence of media or other organic compounds. Furthermore, the powder used in this work (SRM 1898) was free of organic coatings that could potentially undergo sonolytical degradation. This approach is possible with most metal oxides, in which the pH can be adjusted to maximise electrostatic (i.e. surface charge based) stabilisation at low ionic strength levels.

As discussed in the following sections, sonication energy input was calibrated and reported in a transferable manner, and sonication parameters were optimised. The objective of this first set of steps was to produce a highly concentrated aqueous nanoparticle stock via sonication, for further use towards the preparation of dispersions in relevant media. The stock suspension obtained under optimised conditions was then validated for key parameters (PSD, IEP, pH and repeatability for different source lots and concentrations).

Sonication energy calibration

Delivered sonication energy per unit time (power) is a critical parameter in determining not only the final size of the dispersed particles, but also the occurrence of a variety of sonication-initiated physicochemical changes that can significantly affect the properties and behaviour of the dispersed material (Taurozzi et al. 2011c). For this reason, measuring and reporting the sonication power applied in the preparation of dispersions in a manner that allows for replication and transferability is a vital step towards harmonisation of ENM risk assessment and the evaluation of quantitative structure–activity relationships. Yet, a common practice when describing the amount of sonication energy applied to produce ENM dispersions involves either reporting the sonicator's intensity/amplitude setting (e.g. "30% amplitude" or "setting of 7") or reporting the power value shown in the sonicator's digital or analogue display. However, neither of these reporting practices allows for the replication of sonication energy conditions by users having a different sonicator or horn, and the device setting–power relationship is typically nonlinear. Furthermore, even the same sonicator operated using identical settings can deliver different energy levels due to variations in the transducer coupling or deterioration of the tip surface. A comprehensive discussion of the "reproducibility problem" involving current sonication energy reporting practices can be found in the literature (Contamine et al. 1995; Kimura et al. 1996; Mason 1991; Taurozzi et al. 2011c).

To this end, we recently proposed (Taurozzi et al. 2011c) a simple and practical set of steps, based on the calorimetric approach (Mason 1991), for the measurement and calibration of sonication energy delivered to the test sample. The proposed procedure allows for the replication and transference of sonication energy conditions between operators that use different devices. Complete details on the calibration procedure can be found in our previous publications (Taurozzi et al. 2010; Taurozzi et al. 2011c). Representative sonication power values obtained for different settings of the device used in this work are shown in Table I.

Pre-dispersion of ENM powder in purified water

Optimisation of sonication parameters

Sonication parameter optimisation studies were performed by preparing 0.5 mg/mL SRM 1898 aqueous suspensions. The suspensions were prepared by adding 0.025 g of SRM 1898 to a 100 mL, 5 cm diameter glass beaker, to which 50 mL of DI water were then added. The beaker was immersed in an ice water bath that covered the beaker just above the internal water level. The sonicator horn was immersed in the beaker to a depth of ≈ 2.5 cm below the air–suspension interface, the same depth as that used for the calibration procedure.

Sonication power. The first set of optimisation tests was performed by varying the sonication power applied to SRM 1898 aqueous suspensions. For each test, the sonicator's power setting was fixed at a value from 1 to 10 – corresponding to the calibrated power values shown in Table I – and operated in continuous mode for 1 min.

Representative LDS-derived PSD profiles and characteristic size parameters determined for dispersions obtained under different power levels are shown in Figure 1. As seen in Figure 1A, the starting suspension (prior to sonication) exhibited a broad polydisperse and multimodal PSD predominantly in the (1–10) μm range, with a major agglomerated

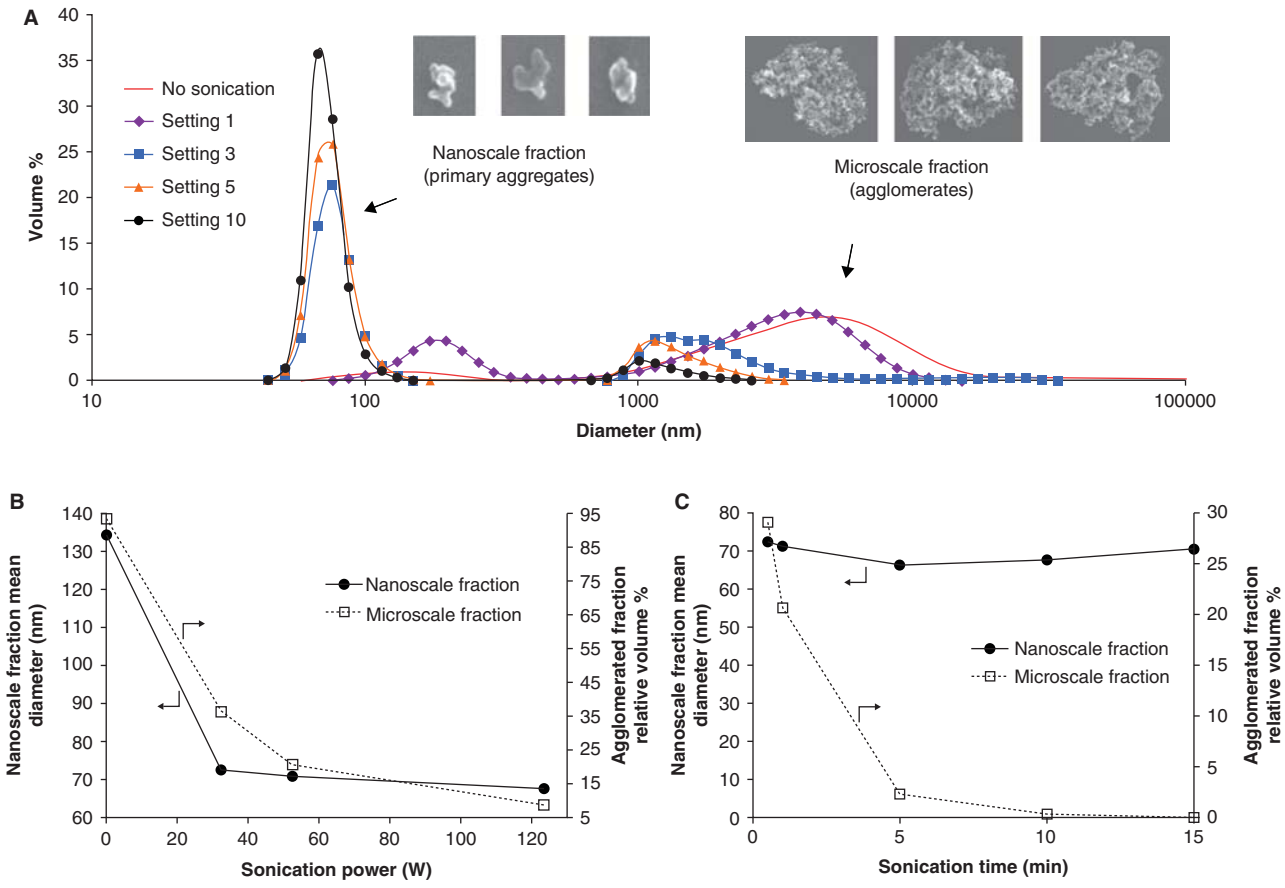

Figure 1. (A) Laser diffraction spectrometry derived particle size distribution profiles of SRM 1898 aqueous suspensions subject to different levels of sonication power for 1 min in continuous mode. Inset micrographs show FE-SEM images of primary aggregates and agglomerates. (B) Nanoscale fraction mean diameter (circles) and agglomerated fraction relative mass (squares) for the dispersions shown in (A). (C) Nanoscale fraction mean diameter (circles) and agglomerated fraction relative mass (squares) for SRM 1898 aqueous suspensions subject to different sonication times at ≈ 50 W in continuous mode for (0–5) min and in 80% pulsed mode for (10–15) min. The sonication power levels associated with specific sonication intensity settings are given in Table I. The arrows in Figures 1B and 1C point to the y-axis corresponding to each plotted trend. SEM micrographs are provided for illustrative purposes and are shown in full detail, including scale bars, in the Supporting Information. Results are presented here to demonstrate optimisation trends; therefore, measurement uncertainties are not stated. Repeatability and uncertainties are evaluated and offered in subsequent sections for the optimised procedure.

fraction (93% of the total particulate volume) centred at around 6 μm and a minor fraction of particles with a peak centred near 130 nm. As the powder in suspension underwent sonication-induced fragmentation, the original PSD profile evolved to a well-defined bimodal distribution, showing a microscale agglomerate fraction with a peak at (1–3) μm and a nanoscale fraction with a peak in the (50–80) nm range. As sonication power was increased, the relative predominance of the microscale fraction decreased, accounting for 20% of the total particulate volume at a sonication power of 50 W (from the original 93% for the un-sonicated suspension). These trends (decrease in nanoscale size fraction characteristic peak value and reduction in the agglomerated microscale fraction) were observed as sonication power increased and in particular at power levels at or above 50 W (Figure 1B). Consistently, two size fractions developed: a nanoscale fraction with a peak mode at ≈ 70 nm and a broader size fraction with a peak near ≈ 1 μm. These two peaks remained relatively unaltered at power values above 50 W. The observed behaviour suggests two configurations for P25 aggregates/agglomerates, wherein the 70 nm peak corresponds to particle clusters we refer to here as *primary aggregates* (see Terminology in SI), while the 1 μm peak suggests that the 70 nm primary aggregates assemble into larger *metastable* agglomerates that tend towards a specific size mode in aqueous suspension (i.e. centred near 1 μm). While the aggregates are presumably fused crystallites resulting from the production process, the agglomerates result from weaker Van der Waals attractive forces and/or a limited number of cleavable contact points. Representative scanning and transmission electron micrographs illustrating the principal morphological characteristics are provided in the Supporting Information.

Sonication time and operation regime. Since the decrease in peak mean size or agglomerated mass fraction was marginal beyond a power of ≈ 50 W as compared with the decrease observed at lower power levels, and higher power settings could potentially result in excessive sample heating and an increased potential for undesirable side effects (Aoki et al. 1987; Vasylkiv & Sakka 2001; Radziuk et al. 2010), a sonicator power setting of 5 (≈ 50 W) was chosen for subsequent optimisation tests (the selected power setting of 5 is specific to the device used in this study; other devices and probe combinations would require calibration as explained previously).

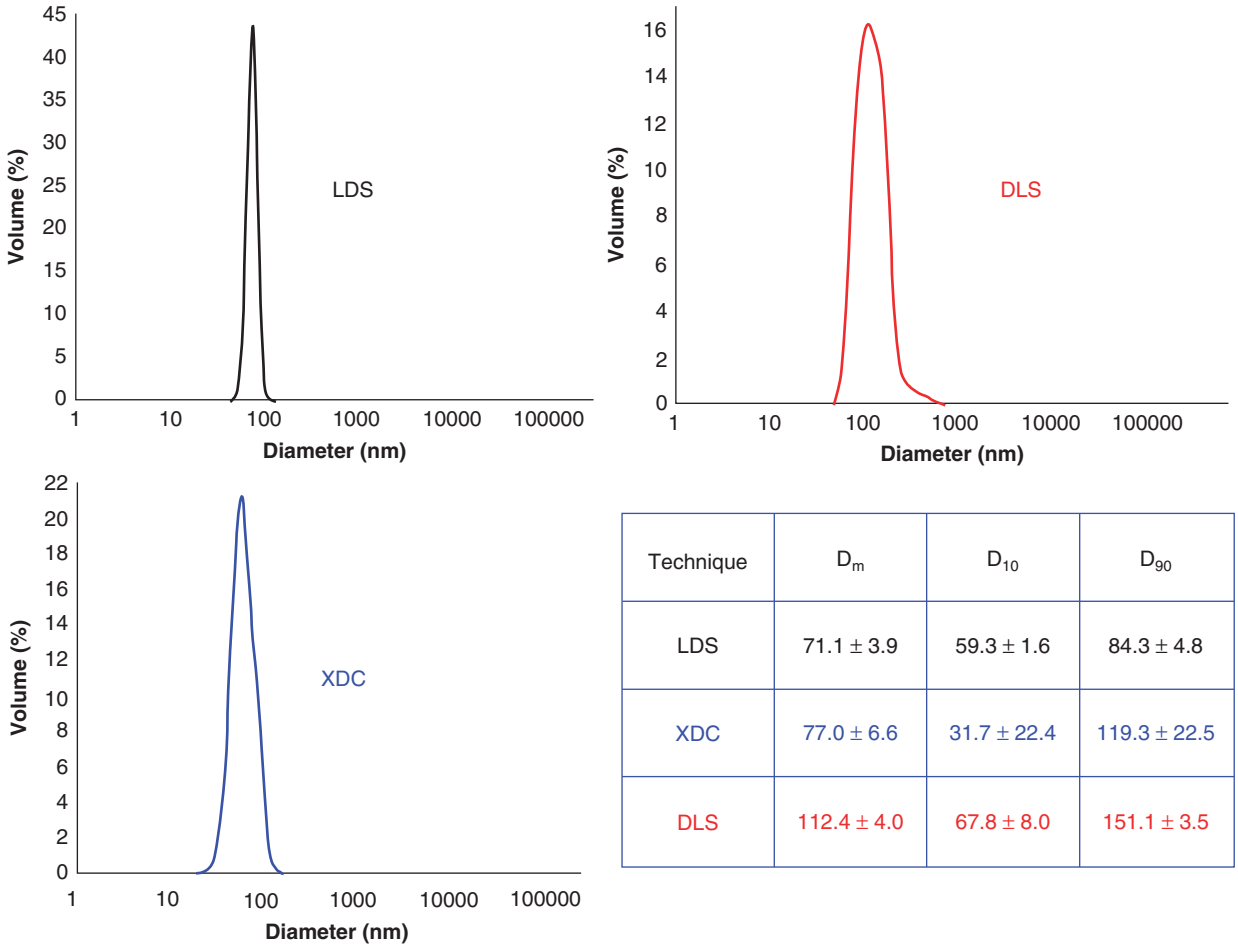

Technique	D_m	D_{10}	D_{90}
LDS	71.1 ± 3.9	59.3 ± 1.6	84.3 ± 4.8
XDC	77.0 ± 6.6	31.7 ± 22.4	119.3 ± 22.5
DLS	112.4 ± 4.0	67.8 ± 8.0	151.1 ± 3.5

Figure 2. Representative particle size distributions obtained by laser diffraction spectrometry (LDS), dynamic light scattering (DLS) and X-ray disc centrifuge (XDC) for 10 mg/mL SRM 1898 dispersions. Table compares the mean size values and associated uncertainties (two standard deviations) for mean (D_m) and cumulative (D_{10} and D_{90}) diameters of SRM 1898 10 mg/mL dispersions determined using the three techniques. Mean values and uncertainties were obtained from the measurement of three independent dispersions with each technique. All dispersions were obtained following the optimised sonication sequence.

Thus, operating at ≈ 50 W in continuous mode, SRM 1898 aqueous suspensions were subject to different sonication times (30 s, 1 min and 5 min). As shown in Figure 1C, increasing the sonication time resulted in a significant decrease in the microscale component volume fraction, while the nanoscale fraction peak position remained relatively unaltered (≈ 70 nm). This trend further confirms that the micrometre-scale peak corresponds to weakly bound agglomerates that can be further fragmented if sufficient energy is delivered, while the 70 nm peak corresponds to "hard" primary aggregates comprising fused crystallites formed during the manufacturing process, which cannot be further disrupted via sonication at the delivered energies. The 70 nm peak therefore represents the smallest achievable particle size for sonicated aqueous dispersions of P25 TiO_2 and SRM 1898, under the conditions tested in this work.

At sonication times above 5 min in continuous mode, the heating of the suspension was appreciable, even when immersed in the ice water bath. For this reason, a pulsed operation mode (rather than the previously used continuous mode) was employed for further optimisation tests. Sonication times of 10 and 15 min were then tested under an 80% pulsation regime (0.8 s on, 0.2 s off). As shown in Figure 1C, at 10 min of sonication, there was still a measurable – though minor – agglomerated component, while at 15 min the microscale component was completely eliminated. Therefore, a sonication time of 15 min and an 80% pulsation mode were selected for further tests.

From the above tests, an optimal set of sonication conditions was obtained for a TiO_2 concentration of 0.5 mg/mL in 50 mL of DI water: sonication power of ≈ 50 W, sonication time of 15 min and an 80% pulsation mode, with a sonication probe immersion depth of 2.5 cm in a cylindrical 100 mL, 5 cm diameter glass beaker. These sonication conditions yielded a narrowly dispersed, monomodal ≈ 70 nm mean particle diameter with no measurable larger size components (Figure 2). A detailed step-by-step protocol for the preparation of SRM 1898 dispersions following the optimised procedure presented herein can be found elsewhere (Taurozzi et al. 2011a).

Validation of optimised sonication sequence

Aqueous nanoparticle stock suspensions obtained by the optimised sonication sequence were subsequently validated by measuring three key parameters critical to nano-EHS studies: PSD, IEP and pH. As discussed in the following

sections, the PSD was measured using three *in situ* techniques to confirm the attainment of a nanoscale and monomodal dispersion (i.e. absence of agglomerates). The IEP and pH were evaluated to establish stability and compatibility considerations in light of the intended use of the stocks as the starting point for the preparation of dispersions in relevant media. Finally, the optimised method was tested for robustness using a variety of P25 lots and over a wide range of initial particle concentrations.

Particle size distribution. LDS, DLS and XDC were used as size characterisation techniques for the validation of the optimised dispersion procedure towards producing aqueous monomodal dispersions in the nanoscale size range. These techniques were selected as they allowed for *in situ* measurements of aqueous nanoscale monomodal dispersions, ensuring statistical robustness and reflecting the state of the particles in their liquid environment with minimal sample transformations. Furthermore, while LDS and DLS measure PSD profiles based on static and dynamic light scattering properties, respectively, XDC provides an additional degree of independence since it relies on fundamentally different principles to determine size (i.e. centrifugal sedimentation coupled with X-ray absorption).

To characterise the PSD of dispersions obtained by the optimised procedure, a triplicate set of 10 mg/mL SRM 1898 aqueous dispersions was prepared following the optimised procedure and then analysed using LDS, DLS and XDC. Unless otherwise noted, all PSD profiles are shown on a volume basis and are thus equivalent to a mass-weighted distribution. Refer to the Supporting Information for definitions of the characteristic size parameters (i.e. mean and cumulative diameters).

Representative PSD profiles and characteristic dimensions for the prepared 10 mg/mL SRM 1898 dispersions measured using the three selected techniques are shown in Figure 2. LDS and XDC yield a statistical match (with respect to the confidence intervals) for the mean diameters and a reasonable consistency with respect to the other characteristic percentiles. By contrast, DLS exhibited statistically larger mean diameter and D_{90} values. In DLS analysis, conversion from an intensity-based to a volume-based PSD necessarily involves a degree of uncertainty due to the inherent low resolution associated with photon correlation analysis and the reliance on a single scattering angle, among other factors. Additionally, DLS measures the equivalent spherical hydrodynamic envelope defined by the primary aggregates' displaced volume, including entrained solution and the hydration shell; thus, the DLS-measured hydrodynamic size is typically larger than a hard core size. As XDC and LDS are orthogonal in nature and less sensitive to the artefacts that impact DLS measurements, these two methods in combination provide validation of the characteristic PSD profile of dispersions prepared following the described procedure. Since LDS requires substantially less sample mass to perform measurements than XDC, it was therefore adopted as the principal size characterisation technique for all subsequent validation tests.

As indicated by the relatively low variation in the measured size parameters, results show a high repeatability for the optimised procedure in terms of yielding consistent PSDs for dispersions obtained from a single P25 production lot (NIST SRM 1898) and at a single particle concentration of 10 mg/mL. This study also shows that DLS can be used to check compliance with the expected dispersion state, so long as other techniques (LDS in this case) are used to optimise and validate the overall approach. As shown in the following sections, further tests were performed to assess the applicability of the procedure for the preparation of dispersions at different particle concentrations and using different P25 production lots.

Repeatability: particle concentration and production lot. Additional validation tests were performed by applying the optimised sonication procedure over a range of particle concentrations (0.5 mg/mL to 20 mg/mL) and for different lots of P25 spanning approximately 20 years of production history. These tests yielded optimal dispersion results (similar to those shown in Figure 2) for all tested concentrations, confirming the robustness and repeatability of the optimised sonication method and the applicability of the approach discussed in this work. A summary of these test results is provided in the Supporting Information.

The stability of the SRM 1898 dispersions prepared following the optimised procedure was measured with respect to the conservation of the PSD profile over time. All prepared dispersions at the tested particle concentrations were stored in capped amber glass vials at room temperature and retained their PSD over 24 h for the lowest tested concentration, while the 10 mg/mL and 20 mg/mL dispersions retained their PSD over 2 weeks. However, since these aqueous dispersions are intended for use as the first step in the preparation of samples in relevant media, they should be used as soon as possible, if not immediately, after preparation. If aqueous suspensions prepared following the recommended sonication procedure are intended for use over longer periods of time, stability should be validated accordingly.

IEP and pH. The prepared aqueous dispersions yielded pH values in the range of 3.7 to 4.9, with dispersions at high particle concentrations exhibiting lower pH values than dispersions at low concentrations (see Supporting Information for representative dispersion pH values as a function of particle concentration). The measured acidic pH values of the as-prepared dispersions are consistent with the manufacturer-reported (Evonik-Degussa 2010) pH values for aqueous P25 dispersions (pH range of 3 to 5) and are explained by the release of protons into the aqueous phase from residual HCl on the surface of the dry powder. The released protons also allow for the electrostatic stabilisation of the nanoparticles in purified water (by shifting the pH away from the IEP), without the need for added stabilising agents. The residual HCl is a by-product of the gas-phase pyrogenic hydrolysis of titanium tetrachloride, which is the basis for the AEROSIL process by which P25 is produced. Accordingly, and as experimentally confirmed, higher P25 concentrations yield lower pH values and longer term

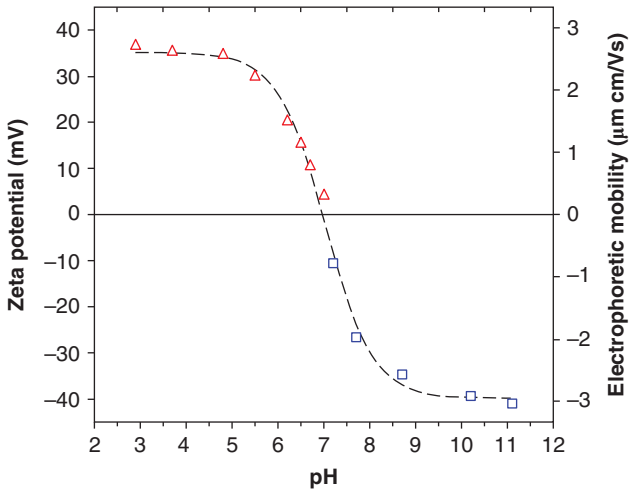

Figure 3. Acidic-to-basic (triangle) and basic-to-acidic (square) titrations showing electrophoretic mobility and zeta potential as a function of pH for SRM 1898 prepared following the prescribed protocol. The dashed line is a five-parameter sigmoidal fit that yields an IEP ≈ 7.0. The standard uncertainty in determining the IEP is estimated to be 0.2 pH units.

stability, due to a greater quantity of protons released into the same volume of medium.

The aqueous dispersions are not intended for use "as is" in toxicological or environmental tests, but instead to be employed as stock suspensions for the preparation of samples in relevant biological or environmental media (as will be subsequently shown). On the other hand, the acidic pH for SRM 1898 aqueous dispersions points to the need for further pH measurements and adjustments, when preparing dispersions in relevant media, in order to ensure that the final pH matches the desired value for the intended assay. The presence of residual HCl on the P25 surface is fortuitous as it ensures that the pH is more than 2 pH units removed from the measured IEP. Other metal oxides, including other TiO_2 test materials, may exhibit a different IEP and may require pH adjustment so as to achieve a stable stock suspension. For instance, P25 is a mixed-phase powder (anatase and rutile polymorphs), whereas a pure phase TiO_2 would likely be characterised by a different IEP (Kosmulski 2002; Kosmulski 2001).

To better understand the stability of dispersions in light of their intended use for the preparation of samples in biological or environmental media, the IEP of SRM 1898 dispersed according to the optimised procedure was evaluated by measuring the electrophoretic mobility (or equivalently, the calculated zeta potential) over an appropriate pH range. Zeta potential values were calculated from the measured electrophoretic mobility at different pH values using the Smoluchowski relationship, which assumes thin double-layer conditions and may not be strictly applicable to particles with a relatively thick electrical double layer and small diameter; however, the absolute magnitude of the zeta potential is not required for the determination of the IEP, and the Smoluchowski value is commonly reported in the literature and is the default setting on many commercial instruments. Therefore, Smoluchowski-derived values are reported in the manuscript for ease of comparison with reported data; the model-independent electrophoretic mobility is also reported. Since pH, zeta potential and IEP are used here within a qualitative stability context, uncertainties are not reported for these values.

The SRM 1898 dispersions used for these tests were prepared at a concentration of 0.5 mg/mL following the optimised procedure. Further experimental details can be found in the Supporting Information. As shown in Figure 3, the titration data yields an estimated IEP at pH ≈ 7, suggesting that the dispersed nanoparticles are most susceptible to agglomeration at physiologically and environmentally relevant pH values (i.e. near neutral pH). This finding emphasises the importance of measuring the stability of the particles in relevant media and adopting measures to control or mitigate agglomeration that can occur due to changes in pH upon introduction into relevant media.

Stabilisation and dispersion in relevant media

Control tests in the absence of stabilising agent

The objective of the first set of tests in relevant media was to determine whether monomodal nanoscale dispersions in the tested media could be prepared by directly mixing the aqueous nanoparticle stock with the biological media of interest (DMEM-FBS or PBS) without a prior stabilisation step. The TiO_2 aqueous stock was thus mixed with each test media, at the same nanoparticle concentration, following two different addition orders: (1) The TiO_2 aqueous stock was pipetted into the medium (addition order 1) or (2) the medium was pipetted to the stock (addition order 2). Further experimental details can be found in the Supporting Information. These tests were conducted in duplicate using independent TiO_2 aqueous stocks for each trial. The resulting samples are referred to as "medium-order #" in Figures 4 and 5.

As shown in Figure 4, mixing the TiO_2 aqueous stock with either medium resulted in the agglomeration of a substantial fraction of the nanoscale primary aggregates, irrespective of the order in which components were mixed. Yet as illustrated by the PSD profiles and the relative volume of agglomerated fractions (Figure 4), a marked difference in the fraction of agglomerated particles was observed for the two mixing orders. That is, adding the aqueous stock into either media resulted in a significantly lower degree of agglomeration than the opposite mixing sequence (medium added to the stock). Additionally, under equal mixing orders, the particles in DMEM-FBS showed a lower degree of agglomeration than those in PBS.

For all cases, the observed agglomeration can be attributed to two factors. First, as discussed previously, the pH of the TiO_2 aqueous stock is ≈ 4, while the pH of the test media is ≈ 7. As shown in Figure 3, the IEP of the TiO_2 nanoparticles in water is at ≈ pH 7, indicating a propensity for agglomeration upon incorporation in the tested media. Moreover, the two test media are rich in ionic species that can screen the surface charge of the nanoparticles, leading to a reduction in the electrostatic repulsive forces that stabilise particles in suspension and causing the observed agglomeration. The instantaneous local concentration of particles (and thus their likelihood of collision and agglomeration) subject to such unfavourable conditions is higher when the media is added into the

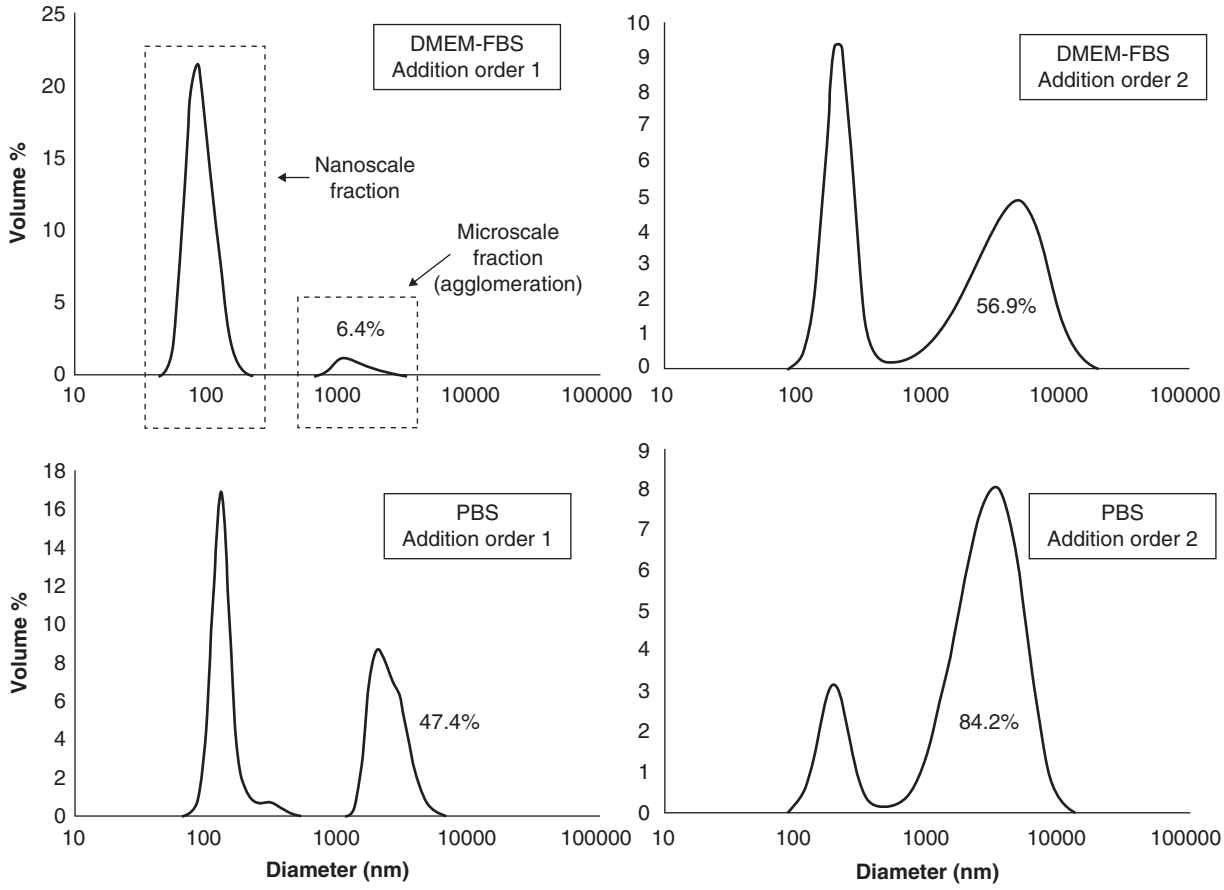

Figure 4. Laser diffraction spectrometry derived particle size distribution profiles of TiO_2 dispersions prepared by mixing an aqueous TiO_2 stock with either DMEM-FBS (top) or PBS (bottom), following two different mixing orders: either the stock was added into the media (order 1, left) or vice versa (order 2, right). In each plot, the relative mass percentage of the agglomerated fraction is shown.

concentrated stock dispersion, as compared with the opposite mixing order, thereby explaining the consistent differences in agglomeration observed for the two mixing orders.

Finally, in the DMEM-FBS case, the medium is also rich in proteins (including BSA), which have been shown to adsorb onto the surface of TiO_2 particles, offering a steric barrier to agglomeration and allowing for particle stabilisation (MacCuspie et al. 2011; Ji et al. 2010; Allouni et al. 2009). The initial excess of proteins with respect to the TiO_2 particles drives protein adsorption onto the particles, mitigating the agglomeration effect produced by unfavourable changes in pH and ionic strength. The presence of proteins in the FBS-enriched DMEM thus explains the reduced extent of agglomeration observed with respect to the protein-free PBS, at identical addition orders. From these tests, three main conclusions can be drawn: (1) The presence of proteins in the receiving medium, in and of itself, does not necessarily prevent agglomeration upon mixing, as all DMEM-FBS suspensions exhibited some degree of agglomeration; (2) proteins can indeed mitigate agglomeration, as shown by the DMEM-FBS vs. PBS comparison using identical addition orders, but the extent to which proteins mitigate agglomeration hinges on the kinetic balance between the effects that favour agglomeration (i.e. pH shift toward the IEP and charge screening) and the effects that mitigate agglomeration (i.e. protein adsorption); and (3) such balance can be affected by the order in which components are mixed, as shown by the differences between the two mixing orders for each test medium.

The performed control tests point to the need for particle stabilisation prior to medium addition in order to avoid agglomeration. A series of optimisation tests were subsequently performed to identify optimal stabilisation conditions using proteins as the stabilising agent. All tests were performed in triplicate using independent TiO_2 stocks for each trial.

FBS vs. BSA as a stabilising agent

FBS is a complex mixture of proteins (BSA being the predominant protein constituent) and other bovine serum components, including ionic species and complex lipids. Given previous reports that indicated that the presence of FBS protected nanoparticles from agglomeration in biological test media (Ji et al. 2010; Allouni et al. 2009; Schulze et al. 2008), the first set of tests was thus a comparative evaluation of FBS and a simple solution of BSA as two possible options for stabilising TiO_2. To this end, 20 mg/mL TiO_2 aqueous stocks were mixed with either (1) a 40 mg/mL BSA aqueous solution or (2) FBS. The concentration of the BSA aqueous solution (40 mg/mL BSA) was chosen so as to match the typical concentration of BSA in FBS. Further experimental details can be found in the supplemental information.

The PSD of the resulting suspensions was characterised using LDS. In all trials, the FBS-treated TiO_2 suspensions showed a significantly larger agglomerated fraction in

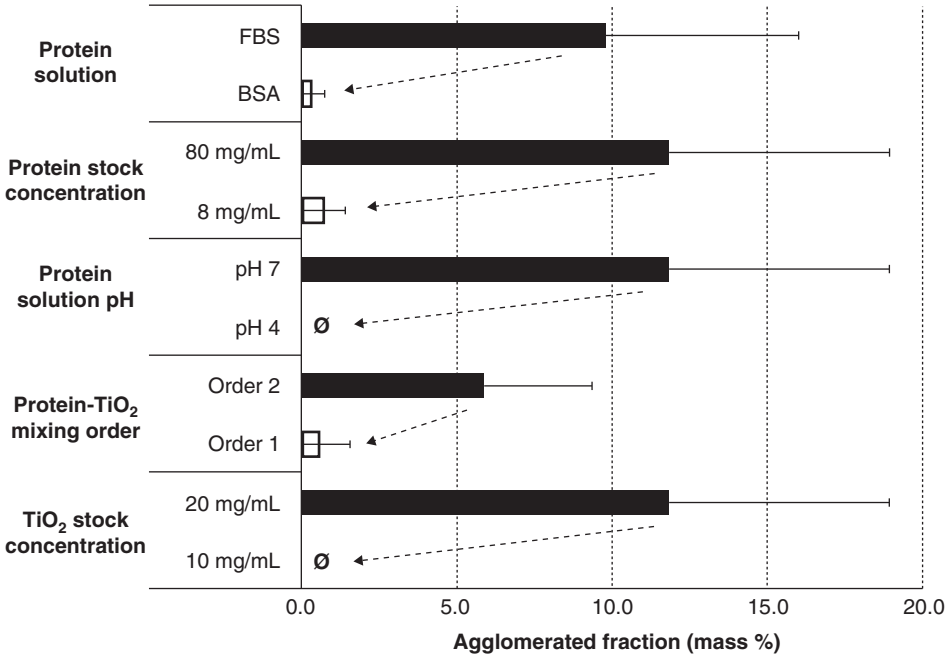

Figure 5. Mass fraction of agglomerated TiO_2 particles in TiO_2–BSA mixtures under different preparation conditions. Each bracketed pair corresponds to a TiO_2-protein mixing condition and its respective control. The "Ø" symbol indicates that no agglomeration was observed for that case.

comparison with their BSA counterparts (Figure 5). As with the medium control tests, the observed agglomeration upon mixing with protein solutions can be explained by a pH shift towards the IEP of the particles (the FBS and BSA solutions have a pH close to 7). Furthermore, at equal BSA concentrations, FBS yielded a greater degree of agglomeration than the BSA solution, due to the additional presence of ionic species in the FBS that are absent in the BSA solution. The additional ionic constituents contribute to charge screening, thus favouring agglomeration. BSA is therefore a more effective stabilising agent than FBS, and BSA aqueous solutions were thus used in all further tests.

BSA and TiO_2 stock concentrations and pH

To evaluate the effect of protein concentration on nanoparticle stability, 20 mg/mL TiO_2 aqueous stocks were mixed with either 8 mg/mL or 80 mg/mL BSA aqueous solutions, while maintaining the same BSA:TiO_2 mass ratio in the final suspensions (further experimental details can be found in the Supporting Information). We refer to the resulting suspensions as "TiO2/BSA-8" or "TiO_2/BSA-80", indicating the respective BSA solution concentrations. As shown in Figure 5, the TiO_2/BSA-80 suspension exhibited a significantly larger agglomerated fraction relative to the TiO_2/BSA-8 suspension.

As with the medium control tests, this observed agglomeration upon mixing with protein solutions can largely be attributed to a pH shift towards the IEP of the particles. The pH of the BSA solutions ranges from 6.8 to 7.1, bracketing the IEP of the test material (SRM 1898) in the aqueous stock. Furthermore, at higher BSA concentrations, the protein solution will have a greater buffering capacity with respect to the post-mixing pH. These results demonstrate that particle stabilisation in protein-rich media is substantially impacted by the concentration of the protein solution *upon mixing*, and not simply by the final BSA:TiO_2 mass ratio. As evidenced, clear differences in agglomeration were observed between the two evaluated cases, in spite of the fact that both samples had the same final BSA:TiO_2 mass ratio.

To demonstrate that the agglomeration effect is pH driven, a subsequent TiO_2/BSA-80 sample was prepared in an identical manner as described above, but the pH of the BSA solution was adjusted to 4 prior to mixing with the TiO_2 stock. As shown in Figure 5, adjusting the pH of the BSA solution away from the IEP of TiO_2 and close to the native pH of the TiO_2 aqueous stock prior to mixing completely eliminated the agglomeration effect. It must be noted, however, that a solution pH of 4 would be inapplicable to most biological tests, and it is simply used here to demonstrate the pH shift hypothesis. Further tests were performed using BSA solutions at their native pH.

It should also be noted that BSA and its species-specific homologues (e.g. HSA, RSA) are rather unique, in that they express a reversible pH-dependent denaturisation that results in a transition from a compact globular structure at neutral pH to an elongated open structure in acidic media. It is thus likely that the BSA configuration at the TiO_2–water interface will differ when the pH changes and/or will adsorb in an unfolded conformation at low pH. These structural variations can impact the adsorption density and may impact the stabilisation properties associated with BSA (Tsai et al. 2011). Furthermore, it may not be possible to acidify other protein solutions in this manner without causing irreversible structural and functional changes to the protein.

An additional triplicate set of tests was conducted to evaluate the effect of the TiO_2 stock concentration on agglomeration upon mixing with protein solutions. An 80 mg/mL BSA aqueous solution was mixed with a 10 mg/mL TiO_2 stock (a 50% reduction compared with

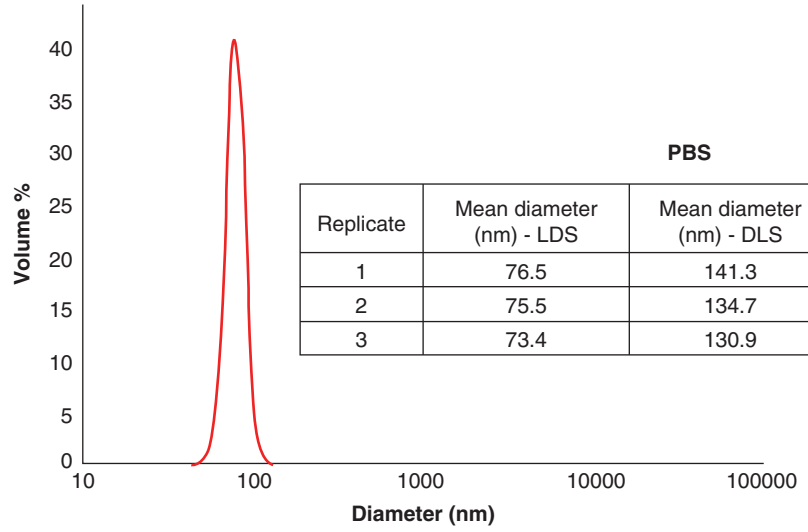

PBS

Replicate	Mean diameter (nm) - LDS	Mean diameter (nm) - DLS	Medium pH	Dispersion PH
1	76.5	141.3	7.3	7.4
2	75.5	134.7	7.3	7.4
3	73.4	130.9	7.3	7.4

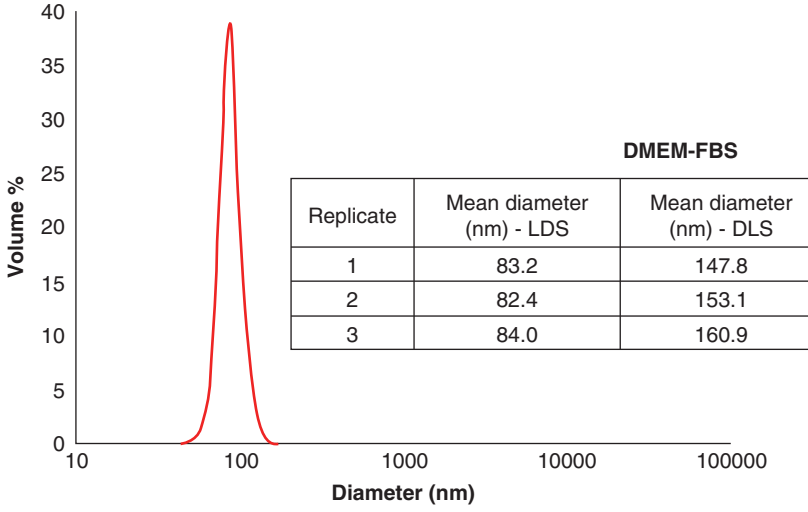

DMEM-FBS

Replicate	Mean diameter (nm) - LDS	Mean diameter (nm) - DLS	Medium pH	Dispersion PH
1	83.2	147.8	7.8	7.8
2	82.4	153.1	7.8	7.8
3	84.0	160.9	7.8	7.8

Figure 6. Representative laser diffraction spectrometry size distribution profiles of TiO_2 dispersions in PBS or DMEM-FBS obtained following the optimised dispersion procedure. Table insets show the respective mean diameters, measured by LDS and dynamic light scattering (DLS), and pH values for three independent replicates.

the 20 mg/mL stock concentration used in previous tests) following mixing order 1. As shown in Figure 5, this modification eliminated the agglomeration previously observed upon mixing with the 80 mg/mL protein solution; in this case, the decrease in collision frequency associated with the lower particle concentration can explain the absence of agglomeration, allowing sufficient time for BSA to saturate the particle surface and thereby impart stability. As expected, the capacity to stabilise nanoparticles improves as particle concentration is decreased.

Nanoparticle–protein mixing order

In this case, a set of tests were performed to determine whether the order in which the TiO_2 stock and protein solution are mixed could affect the state of agglomeration. For this purpose, either a 20 mg/mL TiO_2 stock was added into an 80 mg/mL BSA solution or vice versa. Further experimental details can be found in the Supporting Information. As shown in Figure 5, adding the TiO_2 stock to the BSA solution (order 1) resulted in a consistent reduction of the agglomerated fraction as compared with the opposite sequence (order 2).

As with the medium control tests, when the TiO_2 stock is pipetted into the BSA solution (order 1), there is a large initial protein excess with respect to the added particles, which drives protein adsorption onto the particles as they are incorporated into the medium; this process mitigates the agglomeration effect produced by the unfavourable shift in pH. At the same time, the TiO_2 particles are diluted, thereby reducing interparticle collision frequency. On the other hand, when the BSA solution is added into the TiO_2 stock (order 2), the initial excess of proteins is a localised effect; in this case, the particles appear more prone to pH-driven agglomeration.

Dispersion in biological media

From the above tests, it follows that particle agglomeration upon protein mixing would be affected by the concentration of both the protein and nanoparticle stocks, and the order in which the protein and nanoparticle stocks are mixed.

The final step towards preparing dispersions in the test matrices (PBS and DMEM-FBS) was to determine an optimal protein-to-particle mass ratio that would allow for the stabilisation of the nanoparticles in each medium. Different

BSA:TiO_2 mass ratios were thus evaluated for each medium, following the previously optimised protein mixing conditions (i.e. a TiO_2 stock concentration of 10 mg/mL, a BSA stock concentration of 80 mg/mL and a protein–TiO_2 mixing order wherein the particles are diluted into the protein solution). All tested dispersions were prepared at a TiO_2 upper dose limit concentration of 100 μg/mL. To evaluate different BSA:TiO_2 mass ratios, a fixed volume of a 10 mg/mL TiO_2 aqueous stock was added into different volumes of the 80 mg/mL BSA solution. The resulting aqueous mixtures were then transferred to PBS (1×) or DMEM-FBS (1X) to yield a final particle concentration of 100 μg/mL.

The PSD and pH were determined for the resulting suspensions at different BSA:TiO_2 mass ratios; the selected optimal mass ratios for each medium were those that resulted in the conservation of PSD profiles and pH over the studied 48 h timeframe, while also minimising the amount of added BSA. The evaluated mass ratios, and their characteristic size parameters and agglomerated fractions can be found in the Supporting Information. The optimal BSA:TiO_2 mass ratios, which resulted in no observable agglomeration, were determined to be 16:1 and 1:1 for PBS and DMEM-FBS, respectively. Given its high ionic strength, its strong buffering capacity to a pH close to the particles IEP and the complete absence of proteins, PBS has a much higher tendency to cause nanoparticle agglomeration as compared with DMEM-FBS (as shown in medium control tests). Accordingly, dispersions in PBS required a much higher BSA:TiO_2 mass ratio than in DMEM-FBS to allow for stabilisation.

The PSD of triplicate-independent dispersions obtained using the optimised protein/particle mass ratios for each medium is shown in Figure 6. The optimised procedure consistently yielded monomodal TiO_2 nanoparticle dispersions in both test media, characterised by mean particle diameters of ≈ 75 nm (in PBS) and ≈ 83 nm (in DMEM-FBS), and pH values of 7.4 (in PBS) and 7.8 (in DMEM-FBS). The formulated dispersions were monitored for size and pH over a 48 h period at room temperature in PBS and under incubation conditions of 37°C and 5% CO_2 humidified air in DMEM-FBS. The dispersions retained their PSD and pH over the studied timeframe in all cases; relevant 48 h size parameters for dispersions prepared in both media are offered in the Supporting Information. It must be noted that the pH of the DMEM-FBS dispersion is slightly higher than 7.4 to account for medium acidification during incubation due to the higher CO_2 concentration. A summary of the steps followed to prepare the dispersions in each test media is offered in the Supporting Information, while a detailed step-by-step description of the procedure can be found in (Taurozzi et al. 2011b).

Conclusions

In this work, we demonstrate a transferable and validated approach for the preparation of monodisperse, protein-stabilised TiO_2 nanoparticle dispersions in relevant biological media, intended for acute *in vitro* or *in vivo* toxicity assessment. Studies are conducted using NIST standard reference material 1898, an industrially relevant nanomaterial in powder form. Sonication-induced degradation of stabilisers or medium components is avoided by decoupling the sonication step from the stabilisation and medium addition steps, while sonication power is calibrated and reported in a manner that allows for inter-laboratory transferability. A thorough optimisation of the sonication and protein stabilisation procedures is conducted, to yield a monodisperse nanoparticle aqueous stock characterised and validated for parameters relevant to nanotoxicology (i.e. size distribution, pH, isoelectric point, concentration range, reproducibility and lot-to-lot variability). Under optimised stabilisation conditions and relevant incubation conditions in each medium, the resulting dispersions in the test media remain stable for at least 48 h, retaining their nanoscale particle size distribution and biologically relevant pH values.

While the specific optimised parameters detailed in this document apply to the tested nanomaterial and experimental matrices, we believe that the adopted characterisation, optimisation and validation approaches (i.e. sonication energy calibration, optimisation sequence for particle pre-dispersion, protein stabilisation and medium incorporation steps) can be more generally applied to the preparation of protein-stabilised dispersions in relevant media for other metal oxide ENM powders, with the overall objective of harmonising sample preparation practices that maximise dispersion while minimising sources of artefacts and variability.

Acknowledgements

We thank Fred Klaessig of Pennsylvania Bio Nano Systems, LLC, for helpful suggestions and his critical review of the draft manuscript. We thank John Elliott, NIST Biochemical Science Division, for providing access to an incubator and for providing the DMEM-FBS test media used in this study. We thank Prof. Günter Oberdörster, University of Rochester, for sharing his P25 sample for validation tests. Evonik Industries AG is acknowledged for providing the P25 lot used in the OECD testing program. The authors acknowledge the contributions of Daniel Markwalter for his valuable assistance in conducting experimental tests under the sponsorship of NIST's Summer Undergraduate Research Fellowship (SURF) program, and participants of the International Alliance for NanoEHS Harmonization for many useful discussions, some of which helped motivate the current work.

Declaration of interest

The authors report no conflicts of interest. The authors alone are responsible for the content and writing of the paper.

References

Aggarwal P, Hall JB, McLeland CB, Dobrovolskaia MA, McNeil SE. 2009. Nanoparticle interaction with plasma proteins as it relates to particle biodistribution, biocompatibility and therapeutic efficacy. Adv Drug Deliv Rev 61:428–437.

Allouni ZE, Cimpan MR, Hol PJ, Skodvin T, Gjerdet NR. 2009. Agglomeration and sedimentation of TiO2 nanoparticles in cell culture medium. Colloid Surf B 68:83–87.

Aoki M, Ring TA, Haggerty JS. 1987. Analysis and modeling of the ultrasonic dispersion technique. Adv Ceram Mater 2:209–212.
Basedow AM, Ebert KH. 1979. Effects of mechanical stress on the reactivity of polymers - activation of acid-hydrolysis of dextran by ultrasound. Polym Bull 1:299–306.
Bihari P, Vippola M, Schultes S, Praetner M, Khandoga AG, Reichel CA, et al. 2008. Optimized dispersion of nanoparticles for biological in vitro and in vivo studies. Part Fibre Toxicol 5:14.
Contamine RF, Wilhelm AM, Berlan J, Delmas H. 1995. Power measurement in sonochemistry. Ultrason Sonochem 2:S43–S47.
Evonik-Degussa 2010. Highly dispersed metallic oxides produced by the Aerosil process. Tech Bull 56.
Hackley VA, Clogston JD. 2007. Measuring the size of nanoparticles in aqueous media using batch-mode dynamic light scattering. NIST - NCL joint assay protocol PCC-1. http://ncl.cancer.gov/working_assay-cascade.asp.
Hotze EM, Bottero JY, Wiesner MR. 2010. Theoretical framework for nanoparticle reactivity as a function of Aggregation State. Langmuir 26:11170–11175.
Ji ZX, Jin X, George S, Xia TA, Meng HA, Wang X, et al. 2010. Dispersion and stability optimization of TiO(2) nanoparticles in cell culture media. Environ Sci Technol 44:7309–7314.
Jiang JK, Oberdorster G, Biswas P. 2009. Characterization of size, surface charge, and agglomeration state of nanoparticle dispersions for toxicological studies. J Nanopart Res 11:77–89.
Johnston HJ, Hutchison GR, Christensen FM, Peters S, Hankin S, Stone V. Identification of the mechanisms that drive the toxicity of TiO(2) particulates: the contribution of physicochemical characteristics. Part Fibre Toxicol 2009. 6: 33.
Kawasaki H, Takeda Y, Arakawa R. 2007. Mass spectrometric analysis for high molecular weight synthetic polymers using ultrasonic degradation and the mechanism of degradation. Anal Chem 79:4182–4187.
Kim SC, Chen DR, Qi CL, Gelein RM, Finkelstein JN, Elder A, et al. 2010. A nanoparticle dispersion method for in vitro and in vivo nanotoxicity study. Nanotoxicology 4:42–51.
Kimura T, Sakamoto T, Leveque JM, Sohmiya H, Fujita M, Ikeda S, et al. 1996. Standardization of ultrasonic power for sonochemical reaction. Ultrason Sonochem 3:S157–S161.
Kosmulski M. 2001. Chemical properties of material surfaces. New York: Marcel Dekker.
Kosmulski M. 2002. The significance of the difference in the point of zero charge between rutile and anatase. Adv Colloid Interface Sci 99:255–264.
Krysanov EY, Pavlov DS, Demidova TB, Dgebuadze YY. 2010. Effect of nanoparticles on aquatic organisms. Biol Bull 37:406–412.
Kuempel ED, Ruder A. 2006. Titanium dioxide IARC review monograph 93. Int Agency Res Cancer.
Lin DH, Tian XL, Wu FC, Xing BS. 2010. Fate and transport of engineered nanomaterials in the environment. J Environ Qual 39:1896–1908.
Lundqvist M, Stigler J, Elia G, Lynch I, Cedervall T, Dawson KA. 2008. Nanoparticle size and surface properties determine the protein corona with possible implications for biological impacts. Proc Natl Acad Sci USA 105:14265–14270.
MacCuspie RI, Allen AJ, Hackley VA. 2011. Dispersion stabilization of silver nanoparticles in synthetic lung fluid studied under in situ conditions. Nanotoxicology 5:140–156.
Mason TJ. 1991. Practical sonochemistry: user's guide to applications in chemistry and chemical engineering. Ellis Horwood, Sussex, England.
Naddeo V, Belgiorno V, Napoli RMA. 2007. Behaviour of natural organic mater during ultrasonic irradiation. Desalination 210:175–182.
National Science and Technology Council. 2007. Prioritization of environmental, health and safety research needs for engineered nanoscale materials (An Interim Document for Public Comment). Nanotechnology Environmental and Health Implications Working Group.
National Science and Technology Council. 2008. Strategy for nanotechnology-related environmental, health and safety research. National Science and Technology Council - National Nanotechnology Initiave. http://www.whitehouse.gov/administration/eop/ostp.
NIST. 2012. SRM 1898 was in production as of the publication of this work, and targeted for release in 2011. http://www.nist.gov/srm/.
OECD. 2008. List of manufactured nanomaterials and list of endpoints for phase one of the OECD's testing program, series on the safety of manufactured nanomaterials, Number 6. Paris, France: Environmental Diractorate, Organization for Economic Co-operation and Development.
Pew. 2011. The project on emerging nanotechnologies. Woodrow Wilson International Center for Scholars and the Pew Charitable Trusts. http://www.nanotechproject.org/inventories/consumer/.
Porter D, Sriram K, Wolfarth M, Jefferson A, Schwegler-Berry D, Andrew M, et al. 2008. A biocompatible medium for nanoparticle dispersion. Nanotoxicology 2:144–154.
Radziuk D, Grigoriev D, Zhang W, Su DS, Mohwald H, Shchukin D. 2010. Ultrasound-assisted fusion of preformed gold nanoparticles. J Phys Chem C 114:1835–1843.
Robichaud CO, Uyar AE, Darby MR, Zucker LG, Wiesner M. R. 2009. Estimates of upper bounds and trends in Nano-TiO(2) production as a basis for exposure assessment. Environ Sci Technol 43:4227–4233.
Sager TM, Porter DW, Robinson VA, Lindsley WG, Schwegler-Berry DE, Castranova V. 2007. Improved method to disperse nanoparticles for in vitro and in vivo investigation of toxicity. Nanotoxicology 1:118–129.
Sass J. 2007. Nanotechnology's invisible threat: Small science, big consequences. Nat Resources Defense Counc. http://www.nrdc.org/health/science/nano/nano.pdf.
Schulze C, Kroll A, Lehr CM, Schafer UF, Becker K, Schnekenburger J, et al. 2008. Not ready to use - overcoming pitfalls when dispersing nanoparticles in physiological media. Nanotoxicology 2:51–U17.
Taurozzi JS, Hackley VA, Wiesner MR. 2010. CEINT/NIST Protocol for the preparation of nanoparticle dispersions from powdered material using ultrasonic disruption. http://ceint.duke.edu/allprotocols.
Taurozzi JS, Hackley VA, Wiesner MR. 2011a. CEINT/NIST Protocol for the preparation of a nanoscale TiO2 aqueous dispersion for toxicological or environmental testing. http://ceint.duke.edu/allprotocols.
Taurozzi JS, Hackley VA, Wiesner MR. 2011b. CEINT/NIST Protocol for the preparation of nanoscale TiO2 dispersions in biological test media for toxicological assessment. http://ceint.duke.edu/allprotocols.
Taurozzi JS, Hackley VA, Wiesner MR. 2011c. Ultrasonic dispersion of nanoparticles for environmental, health and safety assessment – Issues and recommendations. Nanotoxicology 5:711–729.
Taylor BN, Kuyatt CE. 1994. Guidelines for Evaluating and Expressing the Uncertainty of NIST Measurement Results, NIST Technical Note 1297. National Institute of Standards and Technology, U. S. Department of Commerce. http://physics.nist.gov/Pubs/guidelines/TN1297/tn1297s.pdf.
Tsai DH, DelRio FW, Keene AM, Tyner KM, MacCuspie RI, Cho TJ, et al. 2011. Adsorption and conformation of serum albumin protein on gold nanoparticles investigated using dimensional measurements and in situ spectroscopic methods. Langmuir 27:2464–2477.
U.S. Environmental Protection Agency, W., DC. 2010. U.S. EPA. Nanomaterial Case Studies: Nanoscale Titanium Dioxide in Water Treatment and in Topical Sunscreen (Final). EPA/600/R-09/057F.
Vasylkiv O, Sakka Y. 2001. Synthesis and colloidal processing of zirconia nanopowder. J Am Ceram Soc 84:2489–2494.
Warheit DB, Webb TR, Reed KL, Frerichs S, Sayes CM. 2007. Pulmonary toxicity study in rats with three forms of ultrafine-TiO2 particles: Differential responses related to surface properties. Toxicology 230:90–104.
Yang XL, Wu JH, Liu W, Xue CB, Zhou SC, Lan FL, et al. 2009. Toxicity and penetration of TiO(2) nanoparticles in hairless mice and porcine skin after subchronic dermal exposure. Toxicol Lett 191:1–8.
Zhang Y, Chen YS, Westerhoff P, Crittenden J. 2009. Impact of natural organic matter and divalent cations on the stability of aqueous nanoparticles. Water Res 43:4249–4257.

Supplementary material available online

Supporting information including definition of terms, test material information, description of equipment, size measurement methods, pH and zeta potential measurement methods, determination of isoelectric point, definition of relevant size parameters, additional validation tests and results, scanning electron micrographs of test material is available online at http://pubs.acs.org.